Acta Cryst. (1972). B28, 60

A Comprehensive X-ray Study of the Ferroelectric-Ferroelastic and Paraelectric-Paraelastic Phases of $Gd_2(MoO_4)_3$

BY WOLFGANG JEITSCHKO

Central Research Department, Experimental Station, E. I. du Pont de Nemours and Company, Wilmington, Delaware* 19898, *U.S.A.*

(*Received* 22 *February* 1971)

The crystal structure of $Gd_2(MoO_4)_3$ has been investigated both at room temperature and at elevated temperatures below and above the ferroelectric-ferroelastic transition temperature (~ 160 °C). Space group, unit-cell dimensions, and formula units per unit cell are: $Pba2$ (C_{2v}^8), $a = 10{\cdot}3881 \pm 0{\cdot}0003$, $b = 10{\cdot}4194 \pm 0{\cdot}0004$, $c = 10{\cdot}7007 \pm 0{\cdot}0006$ Å, $Z = 4$ at 25 °C and $P\bar{4}2_1m$ (D_{2d}^3), $a = 7{\cdot}393 \pm 0{\cdot}002$, $c = 10{\cdot}670 \pm 0{\cdot}004$ Å, $Z = 2$ at 183 °C. Full-matrix least-squares refinements have been carried out with anisotropic thermal parameters with two single-crystal diffractometer data sets measured at 25 and 183 °C, yielding conventional R values of 0·032 (3000 reflections) and 0·028 (880). The high-temperature structure comes close to the average structure of the two ferroelectric-ferroelastic orientations. The differences in interatomic distances between the two modifications are all less than 0·05 Å. Ferroelectric-ferroelastic switching can be accomplished through two macroscopically equivalent switching mechanisms. Changes in interatomic distances of nearest neighbors upon switching are all less than 0·05 Å. The main difference between the two ferroelectric-ferroelastic orientations results through movements of several oxygen atoms by as much as 0·7 Å. The spontaneous polarization was calculated assuming point charges Gd^{3+} and $[MoO_4]^{2-}$ from positional parameters: $P_s = 0{\cdot}175$ μC.cm^{-2}, in good agreement with experiment. Since most of the dipole moments cancel out within the unit cell, $Gd_2(MoO_4)_3$ can be described as a canted antiferroelectric. The temperature dependence of intensities and peak widths of superstructure reflections has been monitored through the transition temperature. Below the transition temperature, temperature-dependent physical properties can be accounted for by gradual changes in positional parameters towards the high-temperature structure. The mechanism of the phase transition is discussed in terms of the 'positional order-disorder' and the 'soft mode' model. The results obtained in the refinement of the room-temperature structure are compared with results of an independent study of this structure by Keve, Abrahams & Bernstein.

Introduction

Since the discovery of the ferroelectric $Gd_2(MoO_4)_3$ (Borchardt, 1963; Borchardt & Bierstedt, 1966), this substance has attracted much interest. It is transparent, colorless, and can be grown in optical-quality boules by the Czochralski technique. Upon cooling, it undergoes a ferroelectric phase transition that has been reported at temperatures between 159 and 163 °C (Borchardt & Bierstedt, 1966; Aizu, Kumada, Yumoto & Ashida, 1969).† Electrical and elastic properties have been reported by: Borchardt & Bierstedt (1967); Cross, Fousková & Cummins (1968); Cummins (1970); Kumada (1969); Epstein, Herrick & Turek (1970). Other reports deal with the temperature-dependent Raman scattering (Fleury, 1970) and the specific heat near the transition temperature (Fousková, 1969). Optical properties (Smith & Burns, 1969; Cummins, 1970) suggest possible applications as light gates. Of further practical interest is the option of switching the material from one orientation to the other, not only by applying an electric field (ferroelectric) but also by applying mechanical stress (ferroelastic behavior; Aizu, 1969). $Gd_2(MoO_4)_3$ is actually the first compound where these properties have been observed simultaneously. Aizu (1970) and Shuvalov (1970) have published comprehensive series of papers dealing with various symmetry aspects of diffusionless phase transitions. To avoid tiring repetitions, some of their abbreviations have been adopted in this paper: the initial, basic, high-symmetry, high-temperature, paraelectric, paraelastic, parent (or reference) phase is called *prototypic phase* (p.p.); the derived, low-temperature, low-symmetry, ferroelectric, ferroelastic phase is designated *ferroic phase* (f.p.).

$Gd_2(MoO_4)_3$ has been characterized with space group $Pba2$ (C_{2v}^8) below, and space group $P\bar{4}2_1m$ (D_{2d}^3) above, the transition temperature by Prewitt (1966). Optical and electrical investigations cited above agree with these results. Reports that did not confirm these findings were discussed by Prewitt (1970), and seem mainly attributable to the failure of recognizing the twinned

* Contribution No. 1792.

† It has been reported (Nassau, Levinstein & Loiacono, 1965; Drobyshev, Frolkina, Ponomarev, Tomashpol'skii, Venevtsev & Zhdanov, 1970; Keve, Abrahams, Nassau & Glass, 1970; Brixner & Bierstedt, 1970) that the phase, as grown from the melt, undergoes a very sluggish, diffusion-controlled phase transition at about 850 °C. Therefore, it should be borne in mind that both modifications of $Gd_2(MoO_4)_3$ discussed in the present paper are metastable below 850 °C. The terms 'high-temperature' and 'low-temperature' phases used in the present paper always correspond to these metastable modifications.

nature of nonpoled crystals. The structure of the subcell of the low-temperature structure has been reported by Abrahams & Bernstein (1966). The full structure of the low-temperature modification was communicated recently (Jeitschko, 1970). Shortly before the present paper was completed, a preprint of an independent study of the low-temperature structure became available (Keve, Abrahams & Bernstein, 1971). A short comparison between the results of the two independent studies is given at the end of the present paper.

Experimental

A poled single-crystal of $Gd_2(MoO_4)_3$ in the form of an elongated prism with rectangular cross section and dimensions $86 \times 104 \times 690\mu$, kindly provided by F. J. Baum, was mounted with its needle axis – which turned out to be the [110] direction – on a glass fiber using M-Bond 610 Adhesive. Buerger precession photographs showed orthorhombic symmetry with the extinctions $0kl$ only with $k=2n$, and $h0l$ only with $h=2n$, thus leading to the two possible space groups $Pba2\,(C_{2v}^8)$ and $Pbam\,(D_{2h}^9)$; the latter can be ruled out because of the noncompatibility of ferroelectricity with a center of symmetry.

Accurate lattice constants were determined through a least-squares refinement of Guinier–Hägg powder data taken at 25°C. High purity KCl ($a=6{\cdot}29310$ Å) obtained from Johnson, Matthey & Co. was used as an internal standard. To insure proper indexing of the powder diagram (Table 1), intensities were calculated

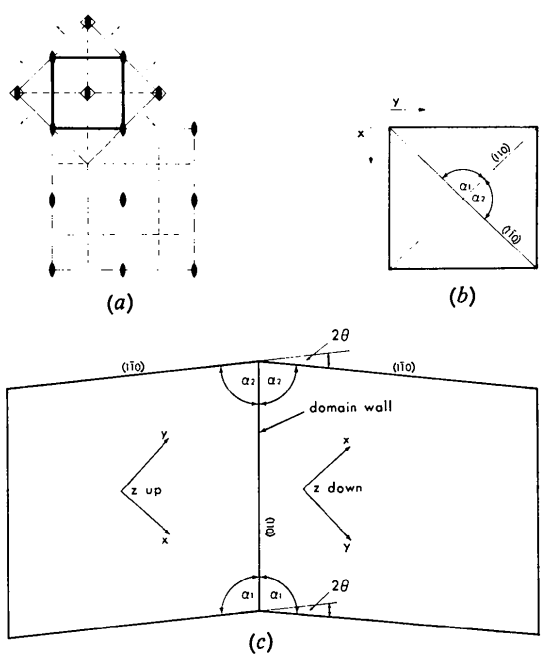

Fig. 1. (*a*) Relation of unit cells of prototypic ($P\bar{4}2_1m$) and ferroic ($Pba2$) $Gd_2(MoO_4)_3$. (*b*) Definition of angles α_1 and α_2. (*c*) Schematic drawing of a single crystal of ferroic $Gd_2(MoO_4)_3$ with two domains, looking down the *c* axis. The {110} planes are cleavage planes and domain walls. Shear angle θ, defined by $\theta=\alpha_1-\alpha_2$, is also the angle between the x direction of one domain and the y direction of the other.

Table 1. *Evaluation of a Guinier–Hägg powder pattern of the ferroic phase* $Gd_2(MoO_4)_3$

Cu $K\alpha$ radiation.

hkl	d_c	d_o	I_c	I_o	hkl	d_c	d_o	I_c	I_o
001	10.7007	10.706	182	s	125	1.9446	-	3	-
110	7.3565	-	< 1	-	215	1.9440	-	< 1	-
111	6.0621	6.064	359	vs	342	1.9400	1.9390	3	vvvw
002	5.3504	5.352	737	vvvs	432	1.9385		4	
020	5.2097	5.210	31	w	250	1.9340	-	2	-
200	5.1941		30		520	1.9298	-	< 1	-
021	4.6841	4.682	472	vvvs	152	1.9087	1.9089	40	w
201	4.6727		476		512	1.9041	1.9039	42	w
120	4.6569	-	4	-	251	1.9032	-	< 1	-
210	4.6485	-	2	-	521	1.8992	-	3	-
112	4.3270	4.327	62	w	044	1.8663	1.8662	25	vvw
121	4.2700	4.267	11	vvvw	404	1.8634	1.8631	23	vvw
211	4.2636		6		225	1.8498	1.8498	55	w
022	3.7325	3.730	411	vvvs	440	1.8391	1.8390	50	w
202	3.7268		406		144	1.8369	-	< 1	-
220	3.6783	3.679	736	vvvs	414	1.8343	-	8	-
003	3.5669	3.568	555	vvs	252	1.8188	-	1	-
122	3.5127	-	13	-	522	1.8153	-	1	-
212	3.5091	-	4	-	441	1.8126	-	5	-
221	3.4785	3.4785	853	vvvs	334	1.8077	-	4	-
130	3.2939	3.2926	560	vvvs	343	1.7979	-	3	-
310	3.2860	3.2867	549	vvvs	433	1.7967	-	3	-
113	3.2095	3.2099	123	m	135	1.7946	1.7940	42	m
131	3.1481	*	84	*	315	1.7933		44	
311	3.1412	*	85	*	350	1.7855	1.7854	203	vs
222	3.0311	3.0314	1000	vvvs	006	1.7835	-	2	-
023	2.9432	2.9419	431	vvvs	530	1.7830	1.7831	205	vs
203	2.9403		416		153	1.7729	1.7727	142	s
230	2.8871	-	< 1	-	513	1.7692	1.7691	139	s
320	2.8838	-	< 1	-	351	1.7611	1.7607	64	w
123	2.8317	-	3	-	531	1.7587	1.7587	58	w
213	2.8298	-	6	-	244	1.7563	1.7556	72	s
132	2.8050	2.8021	294	vvs	424	1.7545		66	
312	2.8001		298		442	1.7392	-	9	-
231	2.7875	-	3	-	060	1.7366	1.7365	58	w
321	2.7845	-	3	-	116	1.7332	-	20	-
004	2.6752	2.6746	79	w	600	1.7314	1.7316	60	w
040	2.6048	2.6043	156	s	235	1.7193	-	< 1	-
400	2.5970	2.5965	153	s	325	1.7186	-	< 1	-
223	2.5606	2.5613	37	vw	061	1.7141	1.7142	30	vw
232	2.5408	-	< 1	-	160	1.7128	-	3	-
322	2.5385	-	< 1	-	601	1.7091	1.7090	32	vw
041	2.5309	2.5306	19	vvw	610	1.7079	-	< 1	-
140	2.5266	-	6	-	253	1.7002	-	1	-
401	2.5238	2.5213	17	vw	523	1.6973	-	1	-
410	2.5199		17		352	1.6937	1.6935	174	s
114	2.5141	-	2	-	532	1.6915	1.6918	162	s
141	2.4590	-	5	-	161	1.6913	-	6	-
411	2.4528	-	4	-	026	1.6873	1.6873	78	s
330	2.4522	-	< 1	-	206	1.6868		75	
133	2.4199	2.4196	60	w	611	1.6866	-	4	-
313	2.4168	2.4171	59	w	126	1.6655	-	1	-
331	2.3902	2.3902	209	vs	216	1.6651	-	2	-
024	2.3798	2.3794	5	vvvw	045	1.6536	1.6530	46	w
204	2.3783		5		062	1.6517	1.6518	114	s
042	2.3420	-	6	-	405	1.6516		47	
402	2.3363	-	6	-	602	1.6473	1.6471	113	m
240	2.3284	2.3279	132	s	260	1.6470	-	< 1	-
420	2.3242	2.3247	135	s	620	1.6430	-	< 1	-
124	2.3197	-	1	-	344	1.6429	-	3	-
214	2.3186	-	2	-	434	1.6420	-	2	-
142	2.2847	-	< 1	-	443	1.6346	1.6345	45	w
412	2.2797	-	5	-	145	1.6330	-	4	-
241	2.2752	2.2747	7	vvvw	162	1.6313	-	7	-
421	2.2713	-	6	-	415	1.6312	-	< 1	-
233	2.2441	-	2	-	261	1.6278	1.6276	67	w
323	2.2426	-	< 1	-	612	1.6270	-	3	-
332	2.2292	-	< 1	-	450	1.6253	-	1	-
224	2.1635	-	< 1	-	540	1.6243	-	< 1	-
005	2.1401	2.1397	19	vvw	621	1.6240	1.6239	62	w
242	2.1350	2.1349	24	vw	154	1.6238	-	1	-
422	2.1318	2.1320	24	vw	514	1.6209	-	1	-
043	2.1036	2.1037	126	s	335	1.6124	1.6125	241	vs
403	2.0995	2.0992	130	s	451	1.6069	-	< 1	-
340	2.0816	2.0824	7	vvvw	541	1.6059	-	1	-
430	2.0799	-	< 1	-	226	1.6048	1.6046	47	w
134	2.0766	2.0761	41	m	353	1.5966	1.5967	58	w
314	2.0746		40		533	1.5948	1.5947	63	w
143	2.0618	2.0617	12	vvvw	245	1.5757	1.5755	79	m
413	2.0581	-	6	-	425	1.5744	1.5743	76	m
115	2.0549	2.0549	80	m	262	1.5741		20	
341	2.0433	-	5	-	622	1.5706	-	22	-
150	2.0432	2.0430	64	w	136	1.5683	1.5680	31	w
431	2.0417	-	5	-	316	1.5675		30	
510	2.0375	2.0374	64	w	254	1.5673	-	1	-
333	2.0207	2.0211	486	vvs	524	1.5651	-	< 1	-
151	2.0069	2.0069	57	w	063	1.5614	-	7	-
511	2.0015	2.0014	56	w	603	1.5576	-	9	-
025	1.9796	1.9790	289	vvs	452	1.5552	-	1	-
205	1.9788		284		542	1.5542	-	3	-
234	1.9623	-	< 1	-	360	1.5523	-	< 1	-
324	1.9612	1.9616	4	vvvw	630	1.5495	-	< 1	-
243	1.9498	1.9493	153	s	163	1.5440	-	1	-
423	1.9473	1.9480	154	s	613	1.5404	-	4	-

* = Coincidence KCl

(Yvon, Jeitschko & Parthé, 1969) using positional parameters from the refined structure. Only clearly resolved lines were included in the least-squares refinement. Lattice constants are: $a = 10{\cdot}3881 \pm 0{\cdot}0003$, $b = 10{\cdot}4194 \pm 0{\cdot}0004$, $c = 10{\cdot}7007 \pm 0{\cdot}0006$ Å, and $V = 1158{\cdot}22 \pm 0{\cdot}14$ Å^3. From these data a shear angle [due to interchange of the a and b axes upon switching; Fig. 1(b) and (c)] of $\theta = 10'\,20'' \pm 15''$ can be calculated, in good agreement with the value of 10·5′ obtained from optical measurements (Cummins, 1970). No evidence of a doubling of the c axis was found in the present investigation (Kvapil & John, 1970). The X-ray density is $D_x = 4{\cdot}555$ g.cm^{-3} with $Z = 4$; measured density was $D_m = 4{\cdot}565 \pm 0{\cdot}005$ g.cm^{-3}.

For the high-temperature single-crystal work, an electrically heated hot-air gun was used that directed a steady stream of hot nitrogen on the crystal and its immediate environment. The temperature was regulated by a rheostat and was calibrated by placing a thermocouple at the position of the crystal after the crystal had been removed. As an additional calibration point, the transition temperature of the crystal was used for which the value of 160°C was chosen from the literature cited above. It was found that the temperature could be held constant within ±2°C over periods of several days.

Buerger precession photographs taken above 160°C are distinguished through the loss of the superstructure reflections.* The symmetry is now truly tetragonal with

* This observation is further specified in a later section of this paper.

Table 2. *Observed and calculated structure factors of the ferroic phase* $Gd_2(MoO_4)_3$

Reading from left to right, the columns contain values h, k, F_{obs}, F_{calc}.

Table 2 (*cont.*)

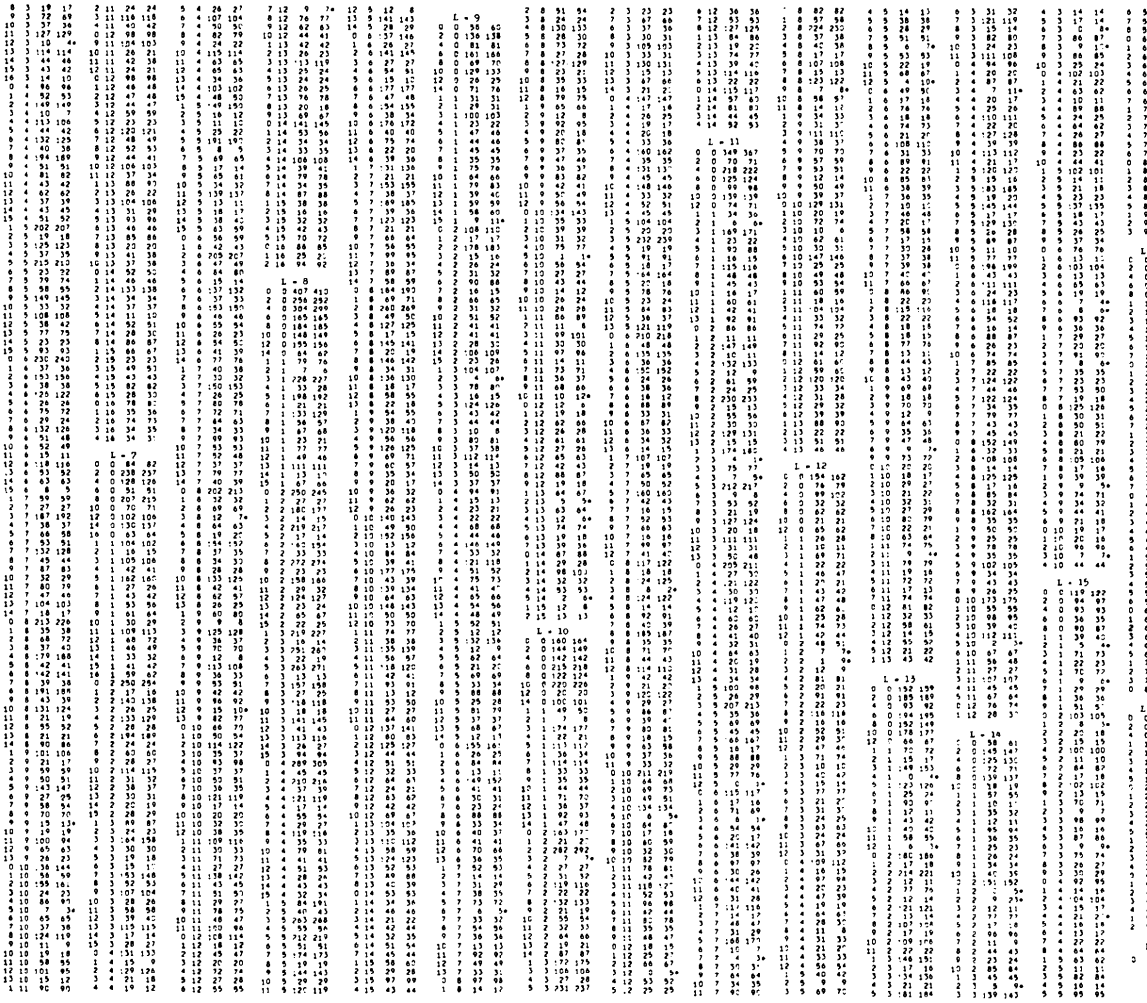

Laue symmetry 4/*mmm*. The only diffraction condition: $h00$ only with $h=2n$ leads to space groups $P42_12$ (D_4^2) and $P\bar{4}2_1m$ (D_{2d}^3). The first one is of point group 422, which is not a supergroup of *mm*2 (the point group of the ferroic phase), and thus could be ruled out (Buerger, 1947).

Lattice constants for the high-temperature structure were obtained from a least-squares refinement of data recorded with a modified MRC high-temperature camera mounted on a Phillips diffractometer. Platinum was used as standard (Esser, Eilender & Bungardt, 1938). At 183 °C (the temperature where single-crystal intensity data for the prototypic phase have been collected) the following lattice constants were obtained: $a=7{\cdot}393\pm0{\cdot}002$, $c=10{\cdot}670\pm0{\cdot}004$ Å, $c/a=1{\cdot}4433\pm0{\cdot}0004$, and $V=583{\cdot}1\pm0{\cdot}2$ Å^3. These agree well with values $a=7{\cdot}38_9$ and $c=10{\cdot}67_5$ Å converted from a diagram in a paper by Newnham, McKinstry, Gregg & Stitt (1969).

X-ray diffraction intensities were collected with an automated Picker single-crystal diffractometer, graphite monochromatized Mo $K\alpha$ radiation, scintillation counter, and pulse-height discriminator. The θ–2θ scan technique was used with a scan speed of 1° 2θ min^{-1} and a scan angle of 1·7° 2θ. Background was counted for 40 sec at the beginning and end of each scan. The intensity of a standard reflection, measured every 5 hr, remained constant within $\pm1{\cdot}5\%$ during the period of data collection. All reflections within one octant up to $(\sin\theta)/\lambda=0{\cdot}86$ (room-temperature structure) and $(\sin\theta)/\lambda=0{\cdot}71$ (high-temperature structure) were collected at temperatures of 25 and 183 °C respectively. Intensities were divided by the angular factor of the monochromator modified Lorentz-polarization correction $\mathrm{Lp}=(\cos^2 2\alpha+\cos^2 2\theta)/(\sin\theta)$, where 2α is the angle between the incident and diffracted beam of a monochromator whose diffracting plane is normal to the diffracting plane of the sample. An absorption correction was made using program *ACACA* written by Prewitt (1967), based on a procedure described by Wuensch & Prewitt (1965). Transmission values found varied between 14·3 and 23·4 %.

Structure refinements

The powder diagram (Table 1) reveals that the tetragonal subcell (only reflections with $h+k=2n$ are strong) is very dominating. The structure of this tetragonal subcell (which corresponds to the average structure of a multiple-domain crystal and, therefore, comes also very close to the high-temperature structure) was solved by Abrahams & Bernstein (1966). An intensity calculation showed that this substructure could well account for all subcell intensities; the atomic positions of the substructure were utilized to initiate positional parameters for least-squares refinements in the orthorhombic low-temperature and tetragonal high-temperature unit cells. To facilitate comparisons between the low- and high-temperature structures, the high-temperature structure was refined in the nonstandard setting $C\bar{4}2_1m$ of space group $P\bar{4}2_1m$, which corresponds to the unit cell of the ferroic phase. General positions for $C\bar{4}2_1m$ are: x, y, z; $\frac{1}{2}-x, \frac{1}{2}-y, z$; $\bar{x}, y, z$; $\frac{1}{2}+x, \frac{1}{2}-y, z$; $y, \frac{1}{2}-x, \bar{z}$; $\frac{1}{2}-y, x, \bar{z}$; $\bar{y}, \frac{1}{2}-x, \bar{z}$; $\frac{1}{2}+y, x, \bar{z}$; $\pm(000, \frac{1}{2}\frac{1}{2}0)$. A full-matrix least-squares program written by Finger (1969) was used. Atomic scattering factors were taken from Cromer & Waber (1965). Corrections for anomalous dispersion were computed with the values given by Cromer (1965). The function min-

Table 3. *Observed and calculated structure factors of the prototypic phase* $Gd_2(MoO_4)_3$

Reading from left to right, the columns contain values h, k. F_{obs}, F_{calc}. Indices correspond to the large low-temperature unit cell.

imized was $\sum w_i(F_o-KF_c)_i^2$, where w_i is the weight based on counting statistics and K is a scale factor. An extinction correction in the form of $I_{corr}=I_{uncorr}/(1-SI_{uncorr})$ was used, where S was $0{\cdot}75\times10^{-6}$.

During the least-squares refinements, it was noticed that the agreement between observed and calculated structure factors was rather poor for several reflections. Some, like reflection 620, were observed as being too strong and could be identified as Renninger reflections by changing the alignment of the crystal (Samson & Gordon, 1968). Others, like reflection 920, were observed as being too weak. In these cases, it turned out that background counts for the reflections had been taken at positions of tails of extremely strong peaks. (The background for the weak peak 920 is affected by the tail of the strong peak 820.) These reflections were marked with an asterisk in the lists of observed and calculated structure factors (Tables 2 and 3), and were not included in the final least-squares cycles. Reflec-

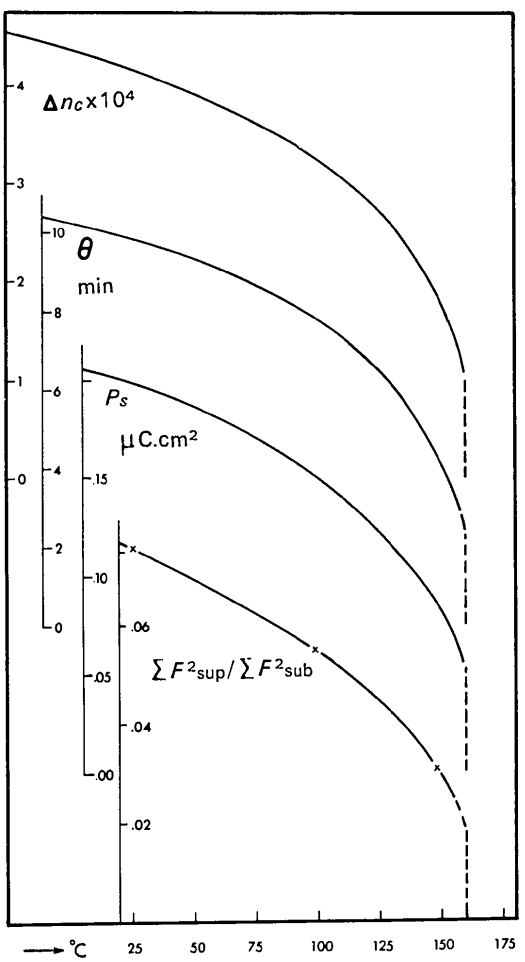

Fig. 2. Temperature dependence of ratio $\sum F^2_{sup}/\sum F^2_{sub}$ as compared to spontaneous polarization P_s, shear angle θ, and spontaneous birefringence Δn_c. Data for P_s, θ, and Δn_c were taken from Cummins (1970). For the behavior of superstructure reflections above T_c, see Fig. 3.

Table 4. *Final positional and thermal parameters of the room-temperature structure of* $Gd_2(MoO_4)_3$

The vibrational parameters ($\times10^5$) are defined through $T=\exp(-\sum_i\sum_j h_i h_j \beta_{ij})$. Numbers in parentheses are e.s.d.'s in the least significant digits. All atoms are in position 4(*c*) of space group *Pba*2.

	x	*y*	*z*	β_{11}	β_{22}	β_{33}	β_{12}	β_{13}	β_{23}	*
Gd(1)	0·18776 (4)	0·49536 (3)	0·73772 (8)	125 (2)	159 (2)	160 (2)	−1 (1)	−11 (2)	− 7 (2)	Gd(1)
Gd(2)	0·49298 (3)	0·31234 (4)	0·26315 (8)	155 (2)	133 (2)	163 (2)	0 (1)	−12 (3)	− 8 (2)	Gd(2)
Mo(1)	0·20569 (6)	0·48898 (5)	0·35726 (10)	109 (4)	154 (4)	172 (4)	2 (3)	9 (3)	−25 (5)	Mo(1)
Mo(2)	0·00289 (5)	0·20649 (7)	0·64257 (11)	164 (4)	121 (4)	182 (4)	−1 (2)	4 (3)	−7 (4)	Mo(2)
Mo(3)	0·24230 (5)	0·24285 (5)	0	178 (4)	183 (4)	129 (4)	−10 (3)	−4 (4)	−13 (4)	Mo(3)
O(1)	0·1921 (10)	0·4882 (8)	0·5186 (9)	505 (73)	819 (88)	273 (58)	31 (51)	119 (52)	−126 (45)	O(9)
O(2)	0·4801 (8)	0·3053 (8)	0·4825 (8)	725 (71)	366 (57)	264 (50)	−63 (50)	−67 (49)	109 (42)	O(10)
O(3)	0·1287 (6)	0·0069 (6)	0·3112 (7)	143 (37)	181 (38)	334 (46)	30 (24)	13 (37)	54 (26)	O(11)
O(4)	0·4940 (5)	0·1280 (7)	0·6899 (7)	202 (41)	203 (41)	322 (47)	−16 (26)	−37 (26)	−45 (39)	O(12)
O(5)	0·1579 (6)	0·1557 (6)	0·6815 (7)	280 (45)	268 (41)	584 (53)	84 (35)	−79 (41)	−77 (42)	O(3)
O(6)	0·1571 (7)	0·3360 (6)	0·3074 (7)	433 (51)	305 (44)	416 (44)	−183 (41)	75 (40)	−195 (39)	O(4)
O(7)	0·3840 (7)	0·3837 (6)	0·7191 (6)	483 (56)	245 (40)	433 (47)	189 (39)	−11 (43)	−41 (36)	O(1)
O(8)	0·3848 (6)	0·1145 (7)	0·2941 (7)	300 (44)	344 (49)	677 (62)	−134 (38)	37 (44)	−6 (45)	O(2)
O(9)	0·1255 (6)	0·1708 (7)	0·0937 (6)	348 (47)	366 (45)	280 (39)	−122 (38)	71 (38)	21 (35)	O(8)
O(10)	0·3174 (7)	0·1264 (7)	0·9074 (7)	499 (58)	307 (46)	372 (48)	53 (41)	−20 (43)	−118 (42)	O(6)
O(11)	0·3545 (7)	0·3197 (7)	0·0984 (6)	372 (51)	582 (62)	228 (41)	−30 (44)	−102 (37)	−91 (40)	O(5)
O(12)	0·1704 (7)	0·3571 (6)	0·9024 (7)	478 (52)	264 (42)	375 (47)	10 (39)	−82 (42)	149 (38)	O(7)

* Atom designation used by Keve, Abrahams & Bernstein (1971).

Table 5. *Final positional and thermal parameters of the high-temperature (at 183 °C) structure of* $Gd_2(MoO_4)_3$

The vibrational parameters ($\times 10^5$) are defined through $T=\exp(-\sum_i\sum_j h_i h_j \beta_{ij})$. Numbers in parentheses are e.s.d.'s in the least significant digits. Parameters are given in terms of the *C*-centered tetragonal unit cell $C\bar{4}2_1$ (D_{2d}^3) which corresponds to the unit cell of the room-temperature structure. The last column contains the designations of point positions in the corresponding standard setting $P\bar{4}2_1m$.

	x	y	z	β_{11}	β_{22}	β_{33}	β_{12}	β_{13}	β_{23}	
Gd(1)	0·18744 (4)	$\frac{1}{4}$	0·73762 (4)	177 (4)	235 (4)	226 (3)	0	−7 (2)	0	4(e)
Mo(1)	0·20663 (8)	$\frac{3}{4}$	0·35695 (7)	161 (6)	245 (6)	261 (6)	0	19 (5)	0	4(e)
Mo(3)	$\frac{1}{4}$	$\frac{1}{4}$	0	277 (6)	277 (6)	172 (7)	0	0	0	2(a)
O(1)	0·1952 (9)	$\frac{1}{2}$	0·5195 (8)	537 (94)	1155 (135)	395 (63)	0	132 (59)	0	4(e)
O(3)	0·1289 (7)	0	0·3109 (6)	276 (58)	295 (61)	363 (51)	0	31 (45)	0	4(e)
O(5)	0·1389 (9)	0·1372 (8)	0·7005 (7)	1061 (93)	838 (81)	1024 (70)	762 (72)	−589 (69)	−285 (64)	8(f)
O(9)	0·1377 (6)	0·1770 (6)	0·0955 (5)	539 (58)	695 (65)	462 (42)	23 (47)	203 (46)	94 (42)	8(f)

tions, where the extinction correction amounted to more than 25%, were treated similarly.

As a check for absolute configuration, several least-squares cycles were run whereby indices *hkl* were changed to $\bar{h}\bar{k}\bar{l}$. The resulting *R* value was 0·046 as compared to $R=0{\cdot}039$ for the correct configuration. Both values correspond to refinements with isotropic temperature parameters.

The accuracy and large number of observed reflections warranted meaningful results for refinements with anisotropic temperature factors. The final *R* values for the structure of the ferroic phase are 0·032 for a total of 3007 reflections and 0·030 for the 2883 reflections included in the last least-squares cycles. For the structure of the prototypic phase, the corresponding values are 0·028 (total of 878 reflections) and 0·027 (864 observed reflections). The corresponding weighted *R* values were 0·054 and 0·046 for the ferroic phase and $R=0{\cdot}038$ and 0·036 for the prototypic phase. Standard deviations of an observation of unit weight were 1·48 and 1·29. Final positional and thermal parameters for the two structures are given in Tables 4 and 5 respectively. The peculiar labeling of atoms in the prototypic phase facilitates identification of corresponding atoms in the ferroic structure (Table 6).

Table 6. *Correspondence of atoms in the high-and low-temperature structures*

High temperature	↔	Low temperature
Gd		Gd(1), Gd(2)
Mo(1)		Mo(1), Mo(2)
Mo(3)		Mo(3)
O(1)		O(1), O(2)
O(3)		O(3), O(4)
O(5)		O(5), O(6), O(7), O(8)
O(9)		O(9), O(10), O(11), O(12)

Dependence of superstructure reflections on temperature

Ferroic phase

As mentioned above, $Gd_2(MoO_4)_3$ has tetragonal symmetry above the transition temperature T_c. Upon cooling through T_c, the symmetry becomes orthorhombic and the unit cell doubles [Fig. 1(*a*)]. In reciprocal space, doubling of the unit cell is characterized by the occurrence of superstructure reflections (reflections with $h+k\neq 2n$ in Table 2). The ratio $\sum F^2_{sup}/\sum F^2_{sub}$, where F_{sup} is a structure factor of the superstructure and F_{sub} is a structure factor of the subcell, is a sensitive indicator for the degree of orthorhombic distortion taking place upon cooling through the transition temperature. Intensity data for the reciprocal lattice plane *hk*0 have been recorded at 25, 98, and 148 °C up to $(\sin\theta)/\lambda=0{\cdot}86$ with the crystal still in the single-domain condition. Fig. 2 shows how the intensities of the superstructure reflections decrease as the temperature approaches the transition temperature. Thus, the ferroic structure transforms to the prototypic

structure gradually. At 140°C, about half the change has already taken place. This corresponds to a similar behavior in other ferroelectric parameters like the spontaneous polarization P_s, spontaneous birefringence Δn_c, and the shear angle θ (Smith & Burns, 1969; Cummins, 1970). The difference between the orthorhombic a and b axes has to decrease in the same way, since it is directly related to the shear angle θ [Fig. 1(*b*) and (*c*)].

Prototypic phase

As the temperature of the crystal approaches T_c, the intensities of the superstructure reflections decrease rapidly, but do not disappear entirely: weak, broad peaks can still be observed at temperatures much higher than T_c. Intensities of these broad peaks, when compared with their intensities below T_c, are uniformly lower and decrease further with rising temperature, while the peak widths are increasing. As an example, intensity data for the superstructure reflections 410+140 and 12,1,0+1,12,0 are plotted in Fig. 3. For comparison, the intensities of the subcell reflections 420 and 12,2,0, which are not affected by the phase transition, are plotted also.

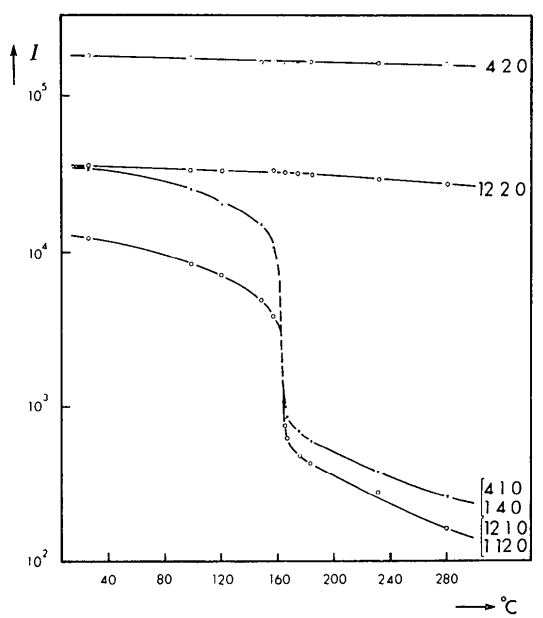

Fig. 3. Intensities of subcell reflections 420 and 12,2,0 and of superstructure reflections (410+140) and (12,1,0+1,12,0) as a function of temperature.

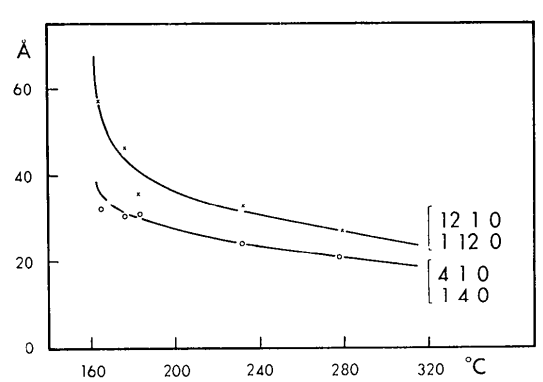

Fig. 4. Apparent particle size as determined from line broadening of the superstructure reflections (410+140) and (12,1,0+1,12,0).

It seems reasonable to interpret these diffuse superstructure peaks as being due to small regions (clusters, fluctuations) of the ferroic low-temperature structure still being present at temperatures above T_c. Making the simplifying (Warren, 1969) assumption that the increase in peak width is due to the decrease in particle size only, and assuming Cauchy shape for the peak profile, one can calculate the diameter of these regions using Scherrer's formula (Scherrer, 1918; Jones, 1938). A correction for instrumental broadening was obtained by measuring the peak half-widths at temperatues below T_c. No further corrections were applied. The results obtained from single-crystal diffractometer scans of the relatively strong peaks 410+140 and 12,1,0+1,12,0 are plotted in Fig. 4. It can be seen that the 'apparent particle size' as calculated from these two peaks is not the same. However, this is not surprising since the 'particles' do not need to be shaped spherically. As discussed later, the 'apparent particle size' can also be understood as the correlation length of amplitudes which are large for low energy ('soft') lattice modes.

Description of the structures

Prototypic phase

There are two symmetry-unrelated Mo atoms and one Gd atom in the structure. Both Mo atoms are tetrahedrally coordinated by oxygen; the Gd atom has seven nearest oxygen neighbors. The four crystallographically different oxygen atoms have either two or three nearest metal atoms.

The structure can be visualized best as being built up from atomic layers perpendicular to the **z** direction. Two layers, at $z \simeq \pm 0{\cdot}3$, are formed by the metal atoms Gd and Mo(1), connected by oxygen atoms O(3) and O(5). These two layers are linked together by oxygen atoms O(1) at $z \simeq 0{\cdot}5$, which each connect a Mo(1) atom of one layer with a Gd atom of the other layer. $[MoO_4]$-tetrahedra formed by Mo(3) and O(9), centered at $z=0$, provide the other link between the layers. A drawing of the high-temperature structure as viewed down the z axis is given in Fig. 5. Program *ORTEP* of Johnson (1965) was used for the structural drawings in this paper. All thermal ellipsoids are drawn at the 50% probability limit.

Ferroic phase

In the low-temperature modification, the symmetry is lower and the volume of the unit cell is doubled. While the temperature is lowered through T_c, the one Gd atom of the high-temperature structure adopts the

environment of either Gd(1) or Gd(2) of the low-temperature structure; Mo(1) of the high-temperature phase becomes Mo(1) or Mo(2) of the low-temperature modification and so on, as summarized in Table 6. Note that the O(5) and O(9) atoms of the high-temperature structure each correspond to four oxygen atoms in the low-temperature modification. Thus, in cocling through T_c, the high-temperature structure has four possibilities for adopting the low-temperature structure. In two of the resultant states, the direction of spontaneous polarization points in the former $+z$ direction of the high-temperature structure and in the other two it points in the $-z$ direction (Fig. 6). Drawings of the low-temperature structure are given in Figs. 7 and 5.

Interatomic distances and angles

The positional parameters (Tables 4 and 5) have been used to calculate interatomic distances (Tables 7 and 8) and angles (Tables 9 and 10) for the ferroic and prototypic modifications. The seven nearest oxygen neighbors around the Gd atoms cover a range from 2·27 to 2·44 Å. Average distances are $2{\cdot}35_4$, $2{\cdot}35_5$, and $2{\cdot}35_4$ Å for Gd(1), Gd(2), and Gd of the low- and high-temperature phases, respectively. It is of interest to compare these distances to the gadolinium–oxygen distances in $Gd_2Si_2O_7$ (Smolin & Shepelev, 1970), where the two crystallographically different Gd atoms also have coordination number 7, which is also found for other rare earth compounds like La_2TiO_5 (Guillen & Bertaut, 1966), $Sm_2Si_2O_7$ (Smolin, Shepelev & Buti-

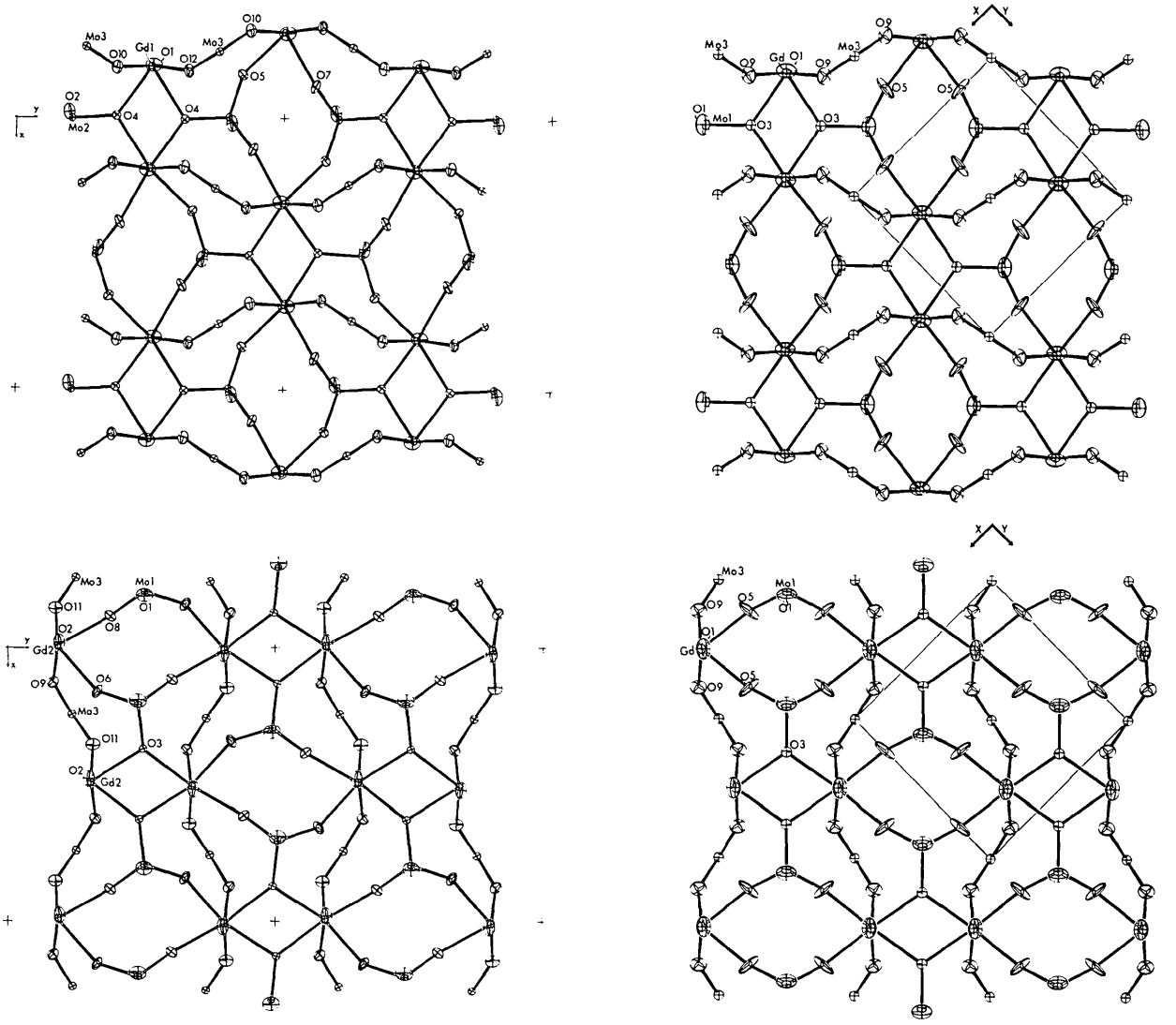

Fig. 5. Comparison of the ferroic (left) and prototypic (right) structure of $Gd_2(MoO_4)_3$. Projection is down the c axis. Upper parts of the drawing correspond to upper parts of the unit cells with atoms at $z \simeq 0{\cdot}7$. Lower parts of the drawings project atoms with $z \simeq 0{\cdot}3$. These layers are linked by O(1) and O(2) atoms at $z \simeq 0{\cdot}5$, which superimpose on Gd(1), Gd(2), Mo(1), and Mo(2). Each partial drawing contains also the projection of one Mo(3) at $z \simeq 0{\cdot}0$ or $z \simeq 1{\cdot}0$ with its linking oxygen atoms O(9), O(11) or O(10), O(12).

kova, 1970), $Er_2Ge_2O_7$ (Smolin, 1970). In $Gd_2Si_2O_7$, the gadolinium–oxygen distances vary between 2·27 and 2·63 Å for one Gd atom and between 2·25 and 2·49 Å for the other. Corresponding average distances are 2·42 and 2·40 Å. The discrepancy of 0·05 Å for these average distances can only be accounted for, in part, by the different coordination numbers of the neighboring oxygen atoms, which average 2·3 Å in $Gd_2(MoO_4)_3$ and 3·1 Å in $Gd_2Si_2O_7$.

The molybdenum–oxygen distances vary less, as revealed in Tables 7 and 8. The average molybdenum–oxygen distances vary between $1{\cdot}73_2$ and $1{\cdot}75_6$ Å, which is somewhat less than the average value of 1·77 Å found for other $[MoO_4]^{2-}$ tetrahedra (Shannon & Prewitt, 1969). The tetrahedral angles in the $[MoO_4]$ tetrahedra vary between 106 and 114°.

Switching mechanisms

$Gd_2(MoO_4)_3$ can be switched either by applying mechanical stress in the [010] or [1$\bar{1}$0] directions (ferro-

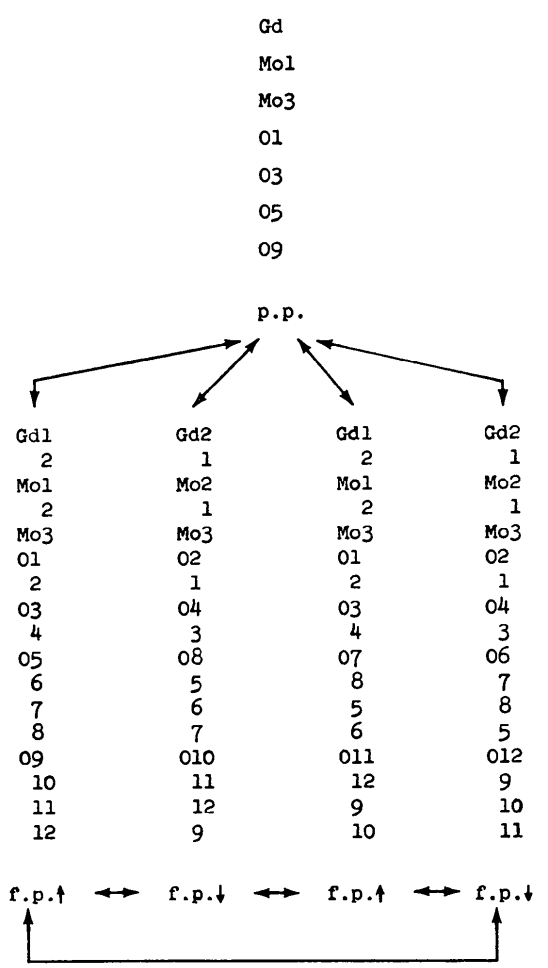

Fig. 6. Scheme showing the four macroscopically equivalent transformations between the ferroic and prototypic phases, and the macroscopically equivalent switching mechanisms between the ferroic states.

Table 7. *Interatomic distances* (Å) *in the structure of ferroic* $Gd_2(MoO_4)_3$

All distances shorter than 3·0 Å are given. Standard deviations are all less than 0·010 Å for metal–oxygen distances and all less than 0·012 Å for oxygen–oxygen distances.

Gd(1)	O(10)	2·272	O(5)	Mo(2)	1·745
	O(12)	2·283		Gd(1)	2·392
	O(1)	2·346		O(4)	2·825
	O(7)	2·356		O(2)	2·848
	O(5)	2·392		O(7)	2·895
	O(4)	2·395		O(7)	2·903
	O(4)	2·442		O(1)	2·917
				O(10)	2·946
Gd(2)	O(11)	2·277			
	O(9)	2·284	O(6)	Mo(1)	1·754
	O(6)	2·349		Gd(2)	2·349
	O(2)	2·351		O(1)	2·783
	O(8)	2·371		O(3)	2·850
	O(3)	2·407		O(8)	2·879
	O(3)	2·443		O(9)	2·881
				O(8)	2·936
Mo(1)	O(1)	1·731			
	O(8)	1·746	O(7)	Mo(2)	1·754
	O(6)	1·754		Gd(1)	2·356
	O(3)	1·800		O(2)	2·841
				O(5)	2·895
Mo(2)	O(2)	1·733		O(5)	2·903
	O(5)	1·745		O(4)	2·915
	O(7)	1·754		O(12)	2·974
	O(4)	1·799			
			O(8)	Mo(10)	1·746
Mo(3)	O(9)	1·743		Gd(2)	2·371
	O(10)	1·750		O(1)	2·853
	O(12)	1·751		O(6)	2·879
	O(11)	1·763		O(3)	2·893
				O(6)	2·936
O(1)	Mo(1)	1·731		O(2)	2·999
	Gd(1)	2·346			
	O(6)	2·783	O(9)	Mo(3)	1·743
	O(8)	2·853		Gd(2)	2·284
	O(3)	2·903		O(11)	2·817
	O(5)	2·917		O(11)	2·840
				O(10)	2·856
O(2)	Mo(2)	1·734		O(12)	2·859
	Gd(2)	2·351		O(6)	2·881
	O(7)	2·841		O(3)	2·887
	O(5)	2·848			
	O(4)	2·891	O(10)	Mo(3)	1·750
	O(8)	2·999		Gd(1)	2·272
				O(12)	2·809
O(3)	Mo(1)	1·800		O(2)	2·847
	Gd(2)	2·407		O(9)	2·856
	Gd(2)	2·443		O(11)	2·895
	O(3)	2·677		O(5)	2·946
	O(6)	2·850		O(4)	2·963
	O(9)	2·887			
	O(8)	2·893	O(11)	Mo(3)	1·763
	O(1)	2·903		Gd(2)	2·277
				O(9)	2·817
O(4)	Mo(2)	1·799		O(9)	2·840
	Gd(1)	2·395		O(12)	2·865
	Gd(1)	2·442		O(10)	2·895
	O(4)	2·669			
	O(5)	2·825	O(12)	Mo(3)	1·751
	O(2)	2·891		Gd(1)	2·283
	O(7)	2·915		O(10)	2·809
	O(12)	2·924		O(10)	2·847
	O(10)	2·963		O(9)	2·859
				O(11)	2·865
				O(4)	2·924
				O(7)	2·974

Table 8. *Interatomic distances* (Å) *in the prototypic structure* $Gd_2(MoO_4)_3$ *at* 183 °C

All distances shorter than 3·0 Å are given. Standard deviations are all less that 0·010 Å for metal-oxygen distances and all less than 0·012 Å for oxygen–oxygen distances.

Gd	2 O(9)	2·293	O(3)	1 Mo(1)	1·787
	1 O(1)	2·330		2 Gd	2·433
	2 O(5)	2·347		1 O(3)	2·695
	2 O(3)	2·433		2 O(5)	2·845
				1 O(1)	2·887
				2 O(9)	2·953
Mo(1)	2 O(5)	1·735	O(5)	1 Mo(1)	1·735
	1 O(1)	1·739		1 Gd	2·347
	1 O(3)	1·787		1 O(1)	2·827
				1 O(3)	2·845
				1 O(5)	2·868
Mo(3)	4 O(9)	1·732		1 O(5)	2·903
				1 O(9)	2·906
				1 O(1)	2·966
O(1)	1 Mo(1)	1·739	O(9)	1 Mo(3)	1·732
	1 Gd	2·330		1 Gd(1)	2·293
	2 O(5)	2·827		1 O(9)	2·800
	1 O(3)	2·887		2 O(9)	2·842
	2 O(5)	2·966		1 O(9)	2·878
				1 O(5)	2·906
				1 O(3)	2·953

elastic switching), or by means of an electric field parallel to the **c** direction (ferroelectric switching). By knowing the point groups of the prototypic and ferroic phases – which differ through the absence of the $\bar{4}$ operation in the ferroic phase – one also knows the orientation of the ferroic domains relative to each other: ferroic switching is accomplished through the $\bar{4}$ operation and, thus, the direction $+\mathbf{a}$ in one domain corresponds to direction $-\mathbf{b}$ in the other domain, $+\mathbf{b}$ corresponds to $+\mathbf{a}$, and $+\mathbf{c}$ to $-\mathbf{c}$. Since the ferroic phase is of a space group possessing glide planes perpendicular to the **a** and **b** directions [Fig. 1(*a*)], one can change the signs of the **a** and **b** directions as long as the origin of the unit cell is shifted accordingly. Thus, it is possible to avoid the inversion operation and the same coordinate system can be used to describe the structure in both orientations. Macroscopically, this amounts to the observation that upon switching, the *a* and *b* axes are interchanged and the *c* axis is inverted, as found experimentally by Smith & Burns (1969), Aizu *et al.* (1969), and Cummins (1970). On the atomic scale, one has to keep in mind that the origin is shifted too, by half a translation period, in either the **a** or **b** direction; thus, one arrives at the two possible switching mechanisms shown in Fig. 8. The left-hand side of Fig. 8 shows the structure in one orientation, the right-hand side in the other (switched) one. The origins in both drawings are marked by an asterisk. The two switching mechanisms can be visualized by superimposing the origin of the left part of Fig. 8 on either point *A* or *B* of the right part. Both mechanisms are equivalent macroscopically. However, on the atomic scale, they are different: *e.g.* O(8) of the left side of Fig. 8 may, upon switching, become atom O(5) and, in doing so, shift by 0·71 Å, or if the other switching mechanism takes place, it becomes O(7) and shifts by only 0·14 Å.

Since each of the two ferroic states has two possibilities to switch to the other state, one arrives at a cyclic process when all possible switching mechanisms are considered, as summarized in Fig. 6. The atom displacements are given in Table 11. In calculating these displacements it was assumed that the orthorhombic *a* and *b* axes have equal length.*

The origins for the superposition in the **z** direction were found using the relation $\sum_i m_i \Delta z_i = 0$, where m_i is the mass and Δz_i is the atomic displacement of atom *i* along the *z* axis. This corresponds to leaving the center of gravity unchanged. The origin of the unit cell, determined by this relation, is only 0·0006 *z*/*c* away from the origin given in Table 4. Table 11 and Fig. 8 show that the displacements are largest for O(6)↔O(7) and O(8)↔O(5). The atoms O(6) and (8) move by

* If $a \neq b$ the two domain lattices cannot be fully superimposed, and displacements depend also on the choice of the matching origins. Atomic displacements of interest are those relative to nearest neighbors. Displacements due to the different lengths of *a* and *b* are a bulk property.

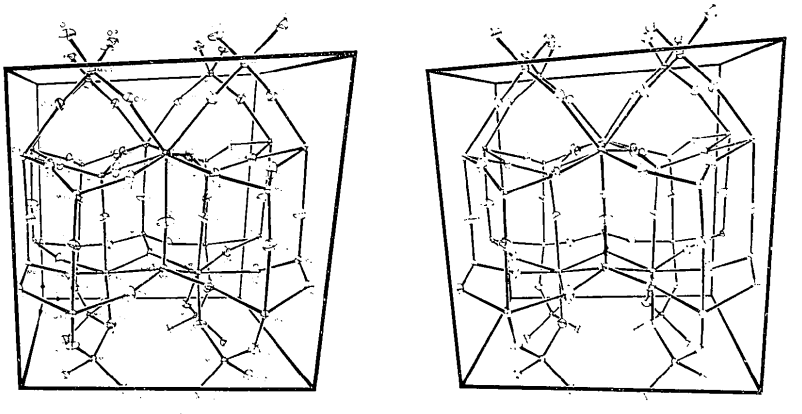

Fig. 7. Stereodiagram of ferroic $Gd_2(MoO_4)_3$.

Table 9. *Interatomic angles* (°) *in the ferroic structure of* $Gd_2(MoO_4)_3$

Standard deviations are all less than 1°.

O(1)—Gd(1)–O(4)	79·6	O(2)—Gd(2)—O(3)	77·7
O(1)—Gd(1)–O(4)	77·8	O(2)—Gd(2)—O(3)	81·1
O(1)—Gd(1)–O(5)	76·0	O(2)—Gd(2)—O(6)	79·6
O(1)—Gd(1)–O(7)	83·3	O(2)—Gd(2)—O(8)	78·9
O(1)—Gd(1)–O(10)	144·9	O(2)—Gd(2)—O(9)	146·0
O(1)—Gd(1)–O(12)	138·8	O(2)—Gd(2)—O(11)	137·5
O(4)—Gd(1)–O(4)	67·0	O(3)—Gd(2)—O(3)	67·0
O(4)—Gd(1)–O(5)	94·1	O(3)—Gd(2)—O(6)	151·5
O(4)—Gd(1)–O(7)	161·6	O(3)—Gd(2)—O(8)	116·5
O(4)—Gd(1)–O(10)	78·8	O(3)—Gd(2)—O(9)	114·5
O(4)—Gd(1)–O(12)	117·8	O(3)—Gd(2)—O(11)	78·9
O(4)—Gd(1)–O(5)	150·1	O(3)—Gd(2)—O(6)	92·7
O(4)—Gd(1)–O(7)	115·8	O(3)—Gd(2)—O(8)	158·1
O(4)—Gd(1)–O(10)	117·7	O(3)—Gd(2)—O(9)	75·9
O(4)—Gd(1)–O(12)	76·4	O(3)—Gd(2)—O(11)	120·6
O(5)—Gd(1)–O(7)	75·1	O(6)—Gd(2)—O(8)	75·2
O(5)—Gd(1)–O(10)	78·3	O(6)—Gd(2)—O(9)	76·9
O(5)—Gd(1)–O(12)	133·4	O(6)—Gd(2)—O(11)	129·6
O(7)—Gd(1)–O(10)	112·6	O(8)—Gd(2)—O(9)	117·6
O(7)—Gd(1)–O(12)	79·7	O(8)—Gd(2)—O(11)	80·7
O(10)—Gd(1)–O(12)	76·2	O(9)—Gd(2)—O(11)	76·3
O(1)—Mo(1)–O(3)	110·6	O(4)—Mo(2)—O(2)	109·8
O(1)—Mo(1)–O(6)	106·0	O(4)—Mo(2)—O(5)	105·7
O(1)—Mo(1)–O(8)	110·2	O(4)—Mo(2)—O(7)	110·2
O(3)—Mo(1)–O(6)	106·6	O(2)—Mo(2)—O(5)	109·9
O(3)—Mo(1)–O(8)	109·3	O(2)—Mo(2)—O(7)	109·1
O(6)—Mo(1)–O(8)	114·0	O(5)—Mo(2)—O(7)	112·1
O(11)—Mo(3)–O(9)	108·2	Mo(2)–O(5)—Gd(1)	152·9
O(11)—Mo(3)–O(10)	111·0		
O(11)—Mo(3)–O(12)	109·2	Mo(1)–O(6)—Gd(2)	150·2
O(9)—Mo(3)–O(10)	109·7		
O(9)—Mo(3)–O(12)	109·8	Mo(2)–O(7)—Gd(1)	155·9
O(10)—Mo(3)–O(12)	109·9		
		Mo(1)–O(8)—Gd(2)	163·7
Gd(1)—O(1)—Mo(1)	175·8		
		Gd(2)–O(9)—Mo(3)	147·5
Gd(2)—O(2)—Mo(2)	168·6		
		Gd(1)–O(10)—Mo(3)	149·2
Gd(2)—O(3)—Gd(2)	107·5		
Gd(2)—O(3)—Mo(1)	117·8	Gd(2)–O(11)—Mo(3)	149·8
Gd(2)—O(3)—Mo(1)	134·4		
		Gd(1)–O(12)—Mo(3)	148·9
Gd(1)—O(4)—Gd(1)	107·5		
Gd(1)—O(4)—Mo(2)	121·4		
Gd(1)—O(4)—Mo(2)	130·8		

Table 10. *Interatomic angles* (°) *in the prototypic phase of* $Gd_2(MoO_4)_3$

Standard deviations are all less than 1°.

O(1)–Gd—O(3)	79·2 (2×)	O(9)–Mo(3)–O(9)	110·3 (6×)
O(1)–Gd—O(5)	78·8 (2×)	O(9)–Mo(3)–O(9)	107·8 (2×)
O(1)–Gd—O(9)	141·1 (2×)		
O(3)–Gd—O(3)	67·2	Gd—O(1)—Mo(1)	177·9
O(3)–Gd—O(5)	104·4 (2×)		
O(3)–Gd—O(5)	157·7 (2×)	Gd—O(3)—Gd	107·2
O(3)–Gd—O(9)	77·2 (2×)	Gd—O(3)—Mo(1)	126·2 (2×)
O(3)–Gd—O(9)	118·3 (2×)		
O(5)–Gd—O(5)	75·2	Gd—O(5)—Mo(1)	164·2
O(5)–Gd—O(9)	77·6 (2×)		
O(5)–Gd—O(9)	123·4 (2×)	Gd—O(9)—Mo(3)	149·4
O(9)–Gd—O(9)	77·8		
O(1)–Mo(1)–O(3)	109·9		
O(1)–Mo(1)–O(5)	108·9 (2×)		
O(3)–Mo(1)–O(5)	107·8 (2×)		
O(5)–Mo(1)–O(5)	113·4		

about 0·7 Å for one switching mechanism: O(6)→O(7) and O(8)→O(5). For the alternate switching mechanism: O(6)→O(5) and O(8)→O(7), the displacements are much smaller. Since the atoms O(6) and O(8) belong to the same atomic layer, one can summarize and distinguish the two mechanisms by saying that either the oxygen atoms of the layer $z \simeq 0{\cdot}3$, or those of the layer $z = 0{\cdot}7$ switch: alternate layers switch. The movements of oxygen atoms during switching in a switching layer are shown in Fig. 9.

Ferroelectric switching involves only minor changes in interatomic distances as seen by a comparison of corresponding interatomic distances using Fig. 6 and Table 7. The largest change in distances of nearest neighbors amounts to 0·043 Å for the change of the distance Gd(1)–O(5) to Gd(2)–O(6). The changes for nearest molybdenum–oxygen distances are all less than 0·013 Å (this is only slightly larger than the limits of accuracy of the present structure determination). Interatomic angles, however, change considerably, especially for the four oxygen atoms O(5) to O(8), which show the largest displacements upon switching.

Since the two switching mechanisms are identical on the macroscopic scale, ferroelectric and ferroelastic switching are completely coupled: partial application of switching stress should lower the switching voltage and partial application of switching voltage should lower the stress needed for switching.

Spontaneous polarization

The spontaneous polarization of $Gd(MoO_4)_3$, reported by various authors cited in the introductory section, varies between 0·17 and 0·20 $\mu C.cm^{-2}$. This value is much smaller than that observed for other ferroelectrics. On the other hand, atomic displacements are similar or even larger in $Gd_2(MoO_4)_3$ than in other ferroelectrics. Abrahams, Kurz & Jamieson (1968) discussed a correlation between average atomic displacements and the value of spontaneous polarization.

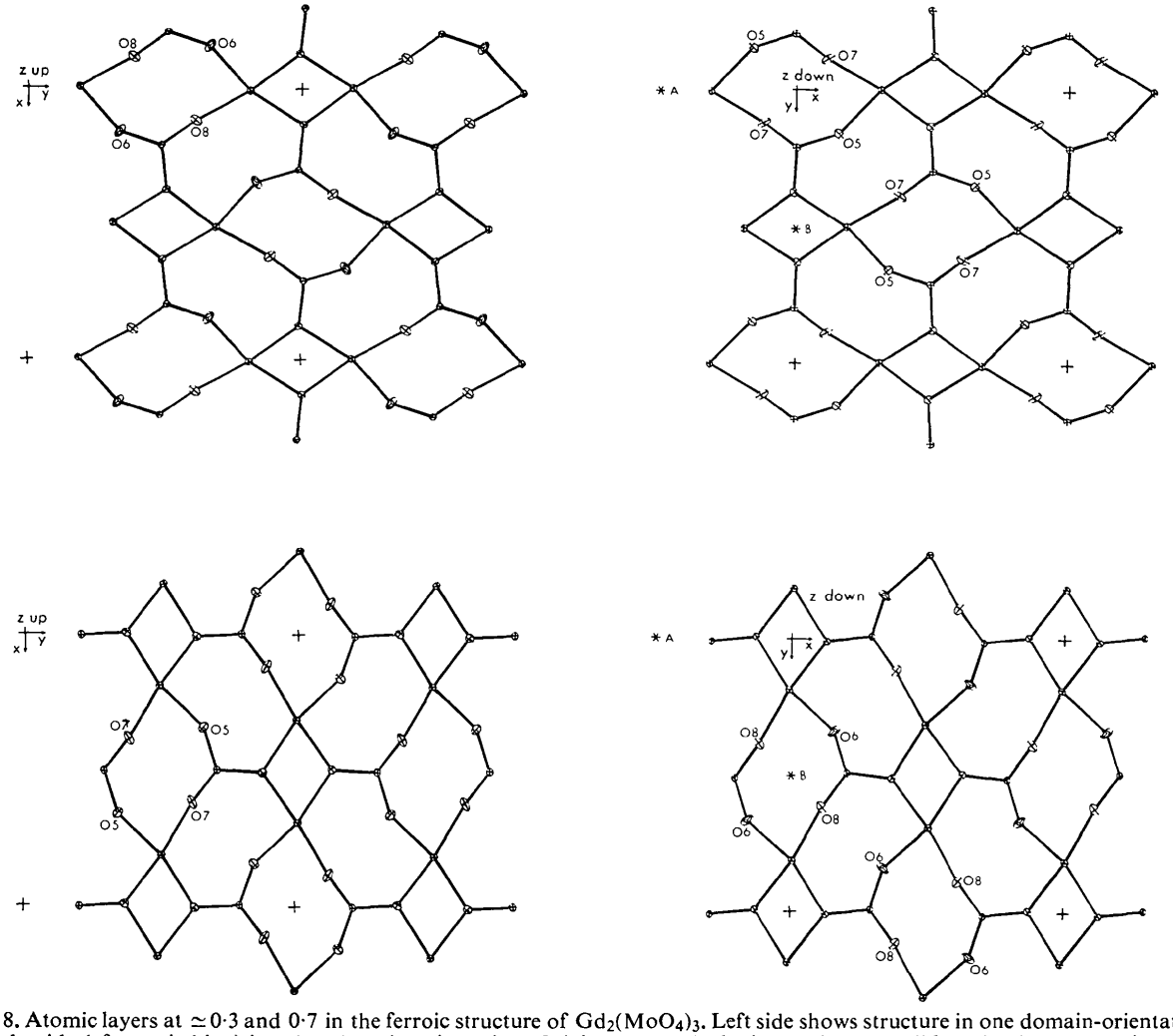

Fig. 8. Atomic layers at $\simeq 0{\cdot}3$ and 0·7 in the ferroic structure of $Gd_2(MoO_4)_3$. Left side shows structure in one domain-orientation, right side (after switching) in other domain orientation. Origins are marked with +. Two possible switching mechanisms can be visualized when the origin of the left-side orientation is superimposed on either point *A* or *B* of the right-side orientation.

According to this correlation, spontaneous polarization should be about 100 times larger than the value actually observed; however, there is no discrepancy. Table 11 shows that large portions of the displacements are in the **a** and **b** directions, which are not contributing to the spontaneous polarization because of the presence of glide planes normal to the **a** and **b** directions in space group *Pba*2. Furthermore, atomic displacements in the **c** direction act mainly against each other. Thus, $Gd_2(MoO_4)_3$ is best described as a *canted antiferroelectric* in analogy to canted antiferromagnetic.

The value of spontaneous polarization can be calculated from positional parameters, assuming full ionization of atoms (Gd^{3+}, Mo^{6+}, O^{2-}) and using the relation $P_s = V^{-1}\sum_i q_i \Delta z_i$, where V is the unit-cell volume, q_i the electric charge, and Δz_i is half the displacement in the z direction during switching of atom i. The summation is taken over all atoms of the unit cell. Alternatively, Δz can also be calculated from the difference between positional parameters of the nonpolar high-temperature structure and the polar low-temperature structure. The resulting value $P_s = 0{\cdot}6 \pm 1{\cdot}6$ μC.cm^2 is small as found experimentally; however, since it results from differences of large numbers, its limits of error are too large. Error limits calculated from standard deviations in positional parameters are mainly attributable to oxygen atoms. Since the oxygen atoms are bound mainly to the molybdenum atoms,* the uncertainties of the positional parameters of the oxygen atoms can be evaded by assuming $[MoO_4]^{2-}$ tetrahedra, with point charges at the Mo position, moving against Gd^{3+} ions. The resulting value, $P_s = 0{\cdot}175 \pm 0{\cdot}080$ μC.cm^2, falls within the range found experimentally.

Accepting that the assumptions made in calculating P_s are valid, the direction of spontaneous polarization is also known, since the absolute configuration of the structure is known: the $+z$ direction points to the face of the crystal with the positive charge.

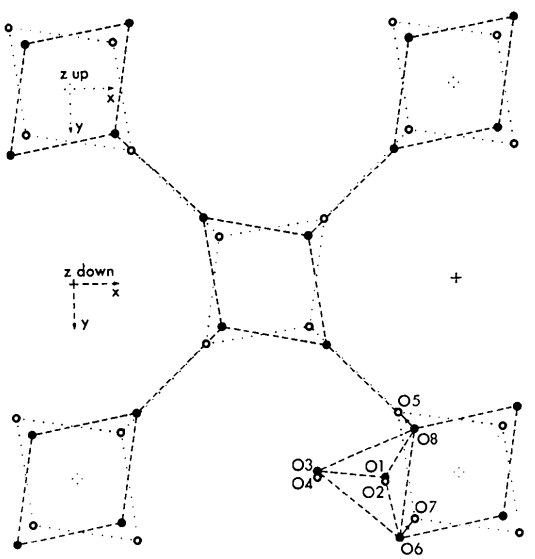

Fig. 9. Displacements of oxygen atoms O(8)→O(5) and O(6)→O(7) during switching. Dotted and broken lines connect atoms of opposite polarity. Oxygen atoms O(1) and O(3), belonging to the same MoO_4-tetrahedron as O(6) and O(8), are only slightly displaced during switching.

Ferroic phase transition

Using Aizu's modified terminology for ferroic phase transitions (Shuvalov, 1970), the ferroic transition of $Gd_2(MoO_4)_3$ can be described with $\bar{4}2m(1)D\bar{4}Fmm2$, where $\bar{4}2m$ and $mm2$ designate point groups of the prototypic and ferroic phases, respectively, (1) means that there is *one* ferroelectric axis, $D\bar{4}$ denotes that it

* This is supported by Raman spectra which show the breathing modes of the $[MoO_4]$ tetrahedra as the dominant features (Shepherd, 1970).

Table 11. *Displacements during switching of* $Gd_2(MoO_4)_3$

Displacement are the same for all transitions between ferroic states shown in Fig. 6.

	Δx (Å)	Δy (Å)	Δz (Å)	Total Δ (Å)
Gd(1) ↔Gd(2)	0·0010	0·0248	0·0030	0·025 ± 0·001
Gd(2) ↔Gd(1)	0·1213	0·0010	0·0030	0·121 ± 0·001
Mo(1) ↔Mo(2)	0·0083	0·1447	0·0081	0·145 ± 0·001
Mo(2) ↔ Mo(1)	0·0846	0·0082	0·0081	0·086 ± 0·001
Mo(3) ↔ Mo(3)	0·1545	0·0057	0·0063	0·154 ± 0·001
O(1) ↔ O(2)	0·027	0·084	0·005	0·09 ± 0·02
O(2) ↔ O(1)	0·329	0·027	0·005	0·33 ± 0·02
O(3) ↔ O(4)	0·007	0·134	0·005	0·13 ± 0·02
O(4) ↔ O(3)	0·009	0·007	0·005	0·01 ± 0·02
O(5) ↔ O(6)	0·063	0·015	0·125	0·14 ± 0·02
O(6) ↔ O(7)	0·424	0·500	0·288	0·71 ± 0·02
O(7) ↔O(8)	0·016	0·012	0·135	0·14 ± 0·02
O(8) ↔ O(5)	0·421	0·452	0·278	0·68 ± 0·02
O(9) ↔ O(12)	0·181	0·004	0·048	0·19 ± 0·02
O(10) ↔ O(9)	0·123	0·009	0·006	0·12 ± 0·02
O(11) ↔ O(10)	0·198	0·024	0·058	0·21 ± 0·02
O(12) ↔ O(11)	0·103	0·027	0·002	0·11 ± 0·02

is defined as parallel to the $\bar{4}$ axis of the initial phase (as opposed to $A\bar{4}$ which symbolizes an arbitrary orientation perpendicular to the former $\bar{4}$ axis), and F designates a ferroic phase and serves mainly to separate adjacent symbols. The presence of the additional symbol ∦ indicates that the direction of spontaneous polarization P_s is reversible, while the symbol itself denotes the non-collinear orientations of lattices with $+P_s$ and $-P_s$ domains.

Diffusionless phase transitions (including ferroelectric transitions) can be classified in two groups: positional order–disorder transitions and displacive transitions. The latter model has been developed extensively during the past decade in terms of an instability of the structure against a vibrational mode (Cochran, 1969), both in theory and experimentally through studies of inelastic neutron scattering and Raman scattering.

The two models can be distinguished through a study of the high-temperature structure. A significant feature of this structure is the apparent anisotropy of thermal motion of oxygen atoms O(5). Apparently, these oxygen atoms vibrate strongly in directions where the corresponding atoms O(5) to O(8) are found upon cooling through the transition temperature. The question arises: is the strongly anisotropic vibration real or is it the result of a least-squares fit for a structure with positional disorder of O(5)? To answer this question, a three-dimensional difference Fourier synthesis for O(5) was computed with $\Delta F = F_{obs}(Gd_2Mo_3O_{12}) - F_{calc}(Gd_2Mo_3O_8)$, using a computer program of Fritchie & Guggenberger (1967). The resulting electron density for O(5) is shown in Fig. 10. Both the 2·0 and 4·0 e.Å^{-3} contours are given in a projection down the tetragonal axis. For comparison, the positions of the corresponding oxygen atoms O(5) to O(8) of the ferroic phase at room temperature are also drawn in. The electron density along a line connecting the average positions O(7) O(8), and O(5) O(6) is also given. If the peak at O(5) of the high-temperature structure resulted from the superposition of two peaks with centers at the average positions O(7) O(8) and O(5) O(6), its electron density at the maximum should be less than, or equal to, 4·8 e.Å^{-3} (4·8 = 1·7 + 3·1, see Fig. 10). Since the actual value is 6·2 e.Å^{-3}, the peak does not result from a superposition of two peaks at the average positions O(7) O(8) and O(5) O(6), and one could conclude that a positional order–disorder transition can be ruled out.

However, these conclusions need to be modified, since the gradual change in structure and physical properties between room temperature and the transition temperature T_c have not been explained yet. As discussed before and as summarized in Fig. 2, about half the change in structure upon heating is accomplished before T_c is reached. Since the positional order–disorder model has already been ruled out (at least concerning the behavior below T_c), there remains only one simple explanation for the gradual change in structure below T_c: when the temperature is raised towards T_c, the oxygen atoms O(5), O(6), O(7), and O(8) move closer to the O(5) position of the prototypic phase (all other atoms move accordingly towards their positions in the high-temperature phase; however, their movements are much smaller and the shifts of oxygen atoms are therefore described as representative for all atoms in the structure). Thus, for the actual phase transition at T_c, the argument given above against the positional order–disorder transition does not hold: the positions of the oxygen atoms O(5) to O(8) just below T_c are much closer to the center of the peak in electron density (Fig. 10) than the room-temperature positions, and the resolution of the peak is not good enough to

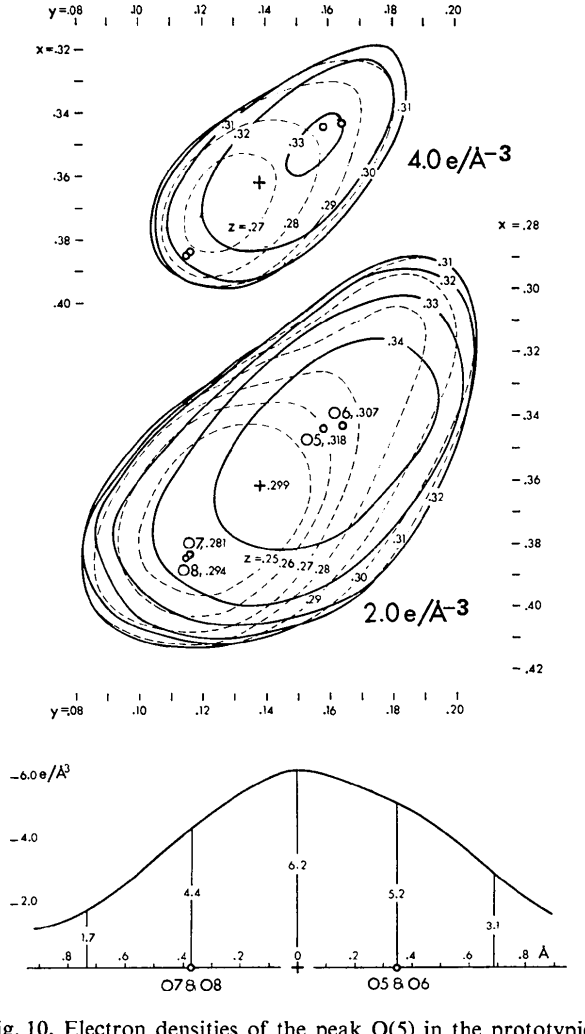

Fig. 10. Electron densities of the peak O(5) in the prototypic structure of $Gd_2(MoO_4)_3$. Contours for 2 and 4 e.Å^{-3} are projected down the z axis. Position of the O(5) atom of the prototypic structure, as obtained through the least-squares refinement, is marked with +. Atomic positions of atoms O(5) to O(8) of the ferroic structure at room temperature are also drawn in. Lowest part shows electron density along a line extending in the directions defined by average positions O(5) & O(6) and O(7) & O(8).

distinguish between a positional order–disorder transition and a lattice dynamical model for the phase transition.

Note that the oxygen atoms O(5) to O(8), which change most during switching, vibrate anisotropically already at room temperature (Fig. 5) with the direction of largest displacement pointing towards the high-temperature O(5) position. As the temperature is raised and their position moves closer towards the high-temperature O(5) position, their amplitude of anisotropic vibration is most likely to increase and the force constant decreases correspondingly. One might speculate whether this vibration corresponds to the soft Raman-active mode observed by Fleury (1970).

While the structural change below T_c is clearly (at least predominantly) displacive, no unambiguous decision between the two models can be made for the final step of the phase transition at T_c based on analysis of the electron-density peak shape. However, further information about the phase transition can be obtained through the behavior of the superstructure reflections. If the high-temperature structure were the result of a statistical positional disorder of the two orientations of the low-temperature structure, integrated intensities of the superstructure peaks should be the same below and above T_c, as has been shown for the positional order–disorder transition in Cu_3Au (Warren, 1969). The dramatic decrease in intensity of the superstructure peaks above T_c indicates that most of the atoms are truly in the high-temperature position, and only a small proportion of the structure participates in the formation of fluctuations in the high-temperature phase. The nature of these fluctuations (positional order–disorder or displacements due to a low-frequency vibrational mode) can only be distinguished through an energy analysis of the scattered radiation. A preliminary result of a neutron diffraction study favors the interpretation in terms of an 'antiferroelectric mode' (Axe, Dorner & Shirane, 1971).

Isotypic rare earth compounds

Borchardt & Bierstedt (1967) reported the rare earth compounds $Sm_2(MoO_4)_3$, $Eu_3(MoO_4)_3$, and $Tb_2(MoO_4)_3$ to be isostructural with $Gd_2(MoO_4)_3$. They also described physical properties, including the ferroic transition temperature, of these compounds. It is well known that the atomic size of the rare earth elements is decreasing with increasing atomic number, as long as the valency is the same. When gadolinium is replaced by the larger elements europium and samarium, the oxygen atoms O(5), O(6), O(7), O(8) of the low-temperature structure are pushed further away from the average O(5) position of the prototypic structure. Thus, the compounds $Sm_2(MoO_4)_3$ and $Eu_2(MoO_4)_3$ need more vibrational energy to reach the transition temperature: their transition temperatures are higher (190 and 161 °C for the Sm and Eu compounds, respectively). On the other hand, the smaller $Tb_2(MoO_4)_3$ has a lower transition temperature (157 °C). Analogous changes should occur in other physical properties.

Comparison of results of two independent studies

As mentioned in the introductory section, the ferroic structure of $Gd_2(MoO_4)_3$ has been studied independently by Keve *et al.* (1971), referred to hereafter as KAB. At the suggestion of reviewers and the Co-editor, some remarks about the similarities and differences of the results of the present study and the KAB one are given here.

The data for the KAB study were collected from a multiple twin crystal. Using normal probability plots (Abrahams & Keve, 1971) KAB found evidence for systematic errors which they ascribed to radiation damage and, in part, to failure in completely accounting for the twinning. In the present study no indication of unusual radiation damage was observed. For comparison purposes, we refined our room-temperature data, as described in the experimental section, with isotropic thermal parameters using the transformed* positional parameters of KAB. The initial R value was $R=0{\cdot}080$ (3007 reflections, unobserved included) and decreased to $R=0{\cdot}039$ in four least-squares cycles. Resultant positional parameters agree all within 2σ of the refinement with anisotropic thermal parameters listed in Table 4. However, the positional parameters found by KAB show a remarkable trend when compared with the parameters found in the present investigation. Parameters that are very similar to the corresponding parameter in the other twin orientation agree well (23 out of 51 positional parameters agree within 3σ of the present investigation). On the other hand, positional parameters that are different from the corresponding parameter in the twin orientation show poor agreement (6 positional parameters differ by as much as 20 to 43 standard deviations of the present investigation or by an average of 8σ of KAB). These relatively large discrepancies in positional parameters do not greatly affect interatomic distances, since the average structure of the twinned crystal comes close to the prototypic structure, and interatomic distances are similar in the ferroic and prototypic structure. For an analysis of the switching mechanisms the greater accuracy of the present study is relevant, since positional parameters of atoms that move most during switching were affected the most by the fact that the data used by KAB were not entirely corrected for twinning.

---

* The parameters given by KAB must be transformed by the pseudosymmetric transformation $(y,x,\frac{1}{2}-z)$ to be compatible with those of the present paper. Although the direction of spontaneous polarization in relation to the crystal structure is identical in both structures, the relationship of the KAB structure to the unit-cell dimensions ($a<b$) is incorrect, as studies of the untwinned crystal show in this investigation. Thus, the direction of the ionic distortions relative to the changes in unit-cell dimensions are different in the two investigations.

The author thanks F. J. Baum for a single-domain crystal of $Gd_2(MoO_4)_3$. Thanks are also due to E. P. Moore, A. D. Foley, and D. M. Graham who gave competent experimental help. The author acknowledges the receipt of the paper by Keve, Abrahams & Bernstein (1971) prior to publication, and expresses his thanks to Drs J. R. Barkley, F. J. Darnell, L. J. Guggenberger, H. S. Jarrett, D. B. Rogers, and I. W. Shepherd for helpful discussions.

References

ABRAHAMS, S. C. & BERNSTEIN, J. L. (1966). *Amer. Cryst. Assn. Winter Meeting*, Abstract N1.

ABRAHAMS, S. C. & KEVE, E. T. (1971). *Acta Cryst.* A**27**, 157.

ABRAHAMS, S. C., KURTZ, S. K. & JAMIESON, P. B. (1968). *Phys. Rev.* **172**, 551.

AIZU, K. (1969). *J. Phys. Soc. Japan*, **26**, 387.

AIZU, K. (1970). *Phys. Rev.* B**2**, 754.

AIZU, K., KUMADA, A., YUMOTO, H. & ASHIDA, S. (1969). *J. Phys. Soc. Japan*, **27**, 511.

AXE, J. D., DORNER, B. & SHIRANE, G. (1971). *Phys. Rev. Lett.* **26**, 519.

BORCHARDT, H. J. (1963). *J. Chem. Phys.* **38**, 1251.

BORCHARDT, H. J. & BIERSTEDT, P. E. (1966). *Appl. Phys. Lett.* **8**, 50.

BORCHARDT, H. J. & BIERSTEDT, P. E. (1967). *J. Appl. Phys.* **38**, 2057.

BRIXNER, L. H. & BIERSTEDT, P. E. (1970). Private communication.

BUERGER, M. J. (1947). *J. Chem. Phys.* **15**, 1.

COCHRAN, W. (1969). *Advanc. Phys.* **18**, 157.

CROMER, D. T. (1965). *Acta Cryst.* **18**, 17.

CROMER, D. T. & WABER, J. T. (1965). *Acta Cryst.* **18**, 104.

CROSS, L. E., FOUSKOVÁ, A. & CUMMINS, S. E. (1968). *Phys. Rev. Lett.* **21**, 812.

CUMMINS, S. E. (1970). *Ferroelectrics*, **1**, 11.

DROBYSHEV, L. A., FROLKINA, I. T., PONOMAREV, V. I., TOMASHPOL'SKII, YU. YA., VENEVTSEV, YU. N. & ZHDANOV, G. S. (1970). *Sov. Phys. Crystallogr.* (Eng. trans.) **15**, 53.

EPSTEIN, D. J., HERRICK, W. V. & TUREK, R. F. (1970). *Solid State Commun.* **8**, 1491.

ESSER, H., EILENDER, W. & BUNGARDT, K. (1938). *Arch. Eisenhüttenw.* **14**, 341.

FINGER, L. W. (1969). Unpublished computer program for the least-squares refinement of crystal structures.

FLEURY, P. A. (1970). *Solid State Commun.* **8**, 601.

FOUSKOVÁ, A. (1969). *J. Phys. Soc. Japan*, **27**, 1699.

FRITCHIE, C. J. & GUGGENBERGER, L. J. (1967). Unpublished electron density summation program.

GUILLEN, M. & BERTAUT, E. F. (1966). *C. R. Acad. Sci. Paris*, **262B**, 962.

JEITSCHKO, W. (1970). *Naturwiss.* **57**, 544.

JOHNSON, C. K. (1965). *ORTEP: A Fortran Thermal-Ellipsoid Plot Program for Crystal Structure Illustrations.* Report ORNL-3794, Oak Ridge National Laboratory, Oak Ridge, Tennessee.

JONES, F. W. (1938). *Proc. Roy. Soc.* A**166**, 16.

KEVE, E. T., ABRAHAMS, S. C. & BERNSTEIN, J. L. (1971). *J. Chem. Phys.* **54**, 3185.

KEVE, E. T., ABRAHAMS, S. C., NASSAU, K. & GLASS, A. M. (1970). *Solid State Commun.* **8**, 1517.

KUMADA, A. (1969). *Phys. Lett.* **30A**, 186.

KVAPIL, J. & JOHN, V. (1970). *Phys. Stat. Sol.* **39**, K15.

NASSAU, K., LEVINSTEIN, H. J. & LOIACONO, G. M. (1965). *J. Phys. Chem. Solids*, **26**, 1805.

NEWNHAM, R. E., MCKINSTRY, H. A., GREGG, C. W. & STITT, W. R. (1969). *Phys. Stat. Sol.* **32**, K49.

PREWITT, C. T. (1966). Cited by BORCHARDT, H. J. & BIERSTEDT, P. E. (1966).

PREWITT, C. T. (1967). Unpublished computer program.

PREWITT, C. T. (1970). *Solid State Commun.* **8**, 2037.

SAMSON, S. & GORDON, E. K. (1968). *Acta Cryst.* B**24**, 1004.

SCHERRER, P. (1918). *Nachr. Göttinger Gesell.* **98**. See WARREN, B. E. (1969). *X-ray Diffraction.* Reading, Massachusetts: Addison-Wesley.

SHANNON, R. D. & PREWITT, C. T. (1969). *Acta Cryst.* B**25**, 925.

SHEPHERD, I. W. (1970). Private communication.

SHUVALOV, L. A. (1970). *J. Phys. Soc. Japan*, **28**, *Supplement*, 38.

SMITH, A. W. & BURNS, G. (1969). *Phys. Lett.* **28A**, 501.

SMOLIN, YU. I. (1970). *Sov. Phys. Crystallogr.* **15**, 36.

SMOLIN, YU. I. & SHEPELEV, YU. F. (1970). *Acta Cryst.* B**26**, 484.

SMOLIN, YU. I., SHEPELEV, YU. F. & BUTIKOVA, I. K. (1970). *Sov. Phys. Crystallogr.* **15**, 214.

WARREN, B. E. (1969). *X-ray Diffraction.* Reading, Massachusetts: Addison-Wesley.

WUENSCH, B. J. & PREWITT, C. T. (1965). *Z. Kristallogr.* **122**, 24.

YVON, K., JEITSCHKO, W. & PARTHÉ, E. (1969). *A Fortran IV Program for the Intensity Calculation of Powder Patterns.* Report of the Lab. for Research on the Structure of Matter, Univ. of Pennsylvania, Philadelphia, Pa.